Delamination of pipeline steels: determination of an anisotropic cleavage criterion

F. TANKOUA[a], J. CREPIN[a], P. THIBAUX[b], M. ARAFIN[b], S. COOREMAN[b], A.F. GOURGUES[a]

[a]*MINES ParisTech, Centre des Matériaux, UMR CNRS 7633, BP87, 91003 Evry cedex, France*
[b]*ArcelorMittal R&D Gent, Pres. J.F. Kennedylaan 3, 9060 Zelzate, Belgium*

Résumé :

L'anisotropie de rupture par clivage a été étudiée sur une tôle d'acier faiblement allié, ferrito-bainitique, pour gazoducs. Des essais mécaniques ont été effectués sur éprouvettes axisymétriques lisses et entaillées dans les trois directions principales de la tôle, pour des températures comprises entre 20°C et -196°C, et analysés par éléments finis à l'aide d'un modèle de plasticité anisotrope. Le mode de rupture dans la direction normale à la tôle diffère de celui dans les deux autres directions, avec une contrainte critique de clivage plus basse. Cette différence est reliée à l'anisotropie de microtexture et pourrait expliquer la sensibilité de cet acier au délaminage à froid.

Abstract:

Cleavage fracture anisotropy has been studied on a ferrite-bainite low alloy pipeline steel plate. Mechanical tests have been performed on smooth and notched bars taken along the three principal directions of the plate at temperatures between 20°C and -196°C, and analyzed by finite element calculations with an anisotropic plasticity model. The fracture mode of specimens tested along the normal direction differs from that of specimens taken along the two other directions, together with a lower critical cleavage stress. This difference seems to be related to microtexture anisotropy and might explain the sensitivity of this steel to delamination at low temperatures.

Keywords: Delamination fracture, anisotropy, cleavage, microtexture, pipeline steels

1 Introduction

Delamination cracking is commonly observed during Charpy or Battelle impact tests on high strength pipeline steels. It involves brittle cracking parallel to the rolling plane and tends to reduce the steel toughness at low temperatures [1-3]. Many authors [1-11] have investigated possible causes and effects of delamination on the mechanical properties of steels. Delamination fracture has been attributed to texture and microstructure anisotropy. It seems to be more pronounced for temperatures within the ductile-to-brittle transition but there is no agreement on the effect of delamination as there are only scarce results on delamination initiation and the interaction of delamination cracks with the main crack propagation. Kalyanam [12] investigated the stress state induced by a static delamination crack in Al-Li alloys, but with no initiation criterion for that crack. Baldi [13] showed that delamination in low alloy steels occurs when the stress along the normal direction (ND) of the plate exceeds a critical value, which is lower than the critical cleavage stress along the rolling (RD) and long transverse (TD) directions. This difference was attributed to shape anisotropy of ferrite grains. The present study aims at providing an anisotropic critical cleavage stress criterion in relation with microstructural parameters, to be used for the modeling of delamination crack initiation. Tensile tests on smooth and notched bars from a pipeline steel plate have been performed at various temperatures, followed by an investigation of the fracture mechanisms. An anisotropic yield criterion has been set to analyze the tests and to derive a value for the critical cleavage stress along RD, TD and ND, and was related to microtexture anisotropy of the plate.

2 Experimental procedure

2.1 Material

A 19.5-mm thick, ferritic-bainitic plate obtained after thermomechanical controlled processing was used (Fig. 1a). It is a micro-alloyed low carbon manganese steel. Its 0.2% proof stress, tensile strength and fracture elongation at room temperature are respectively 580 MPa, 640 MPa, and 42%.

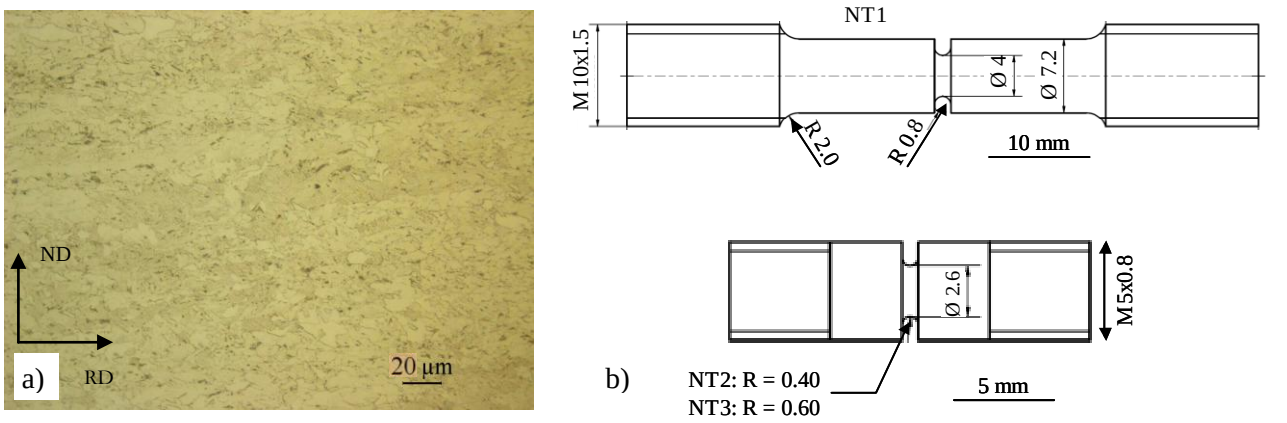

FIG. 1 – (a) Optical micrograph of the steel. (b) Geometry of NT1 (top), NT2 and NT3 (bottom) specimens.

2.2 Mechanical tests

Tensile tests on smooth and notched specimens have been performed by using a 250kN servohydraulic Instron 8500 machine. Cooling was ensured using a climate chamber, except for the tests performed at -196°C; temperature was controlled using a thermocouple spot-welded on the top of the specimen. Tests at -196°C were performed in liquid nitrogen. Two (resp. three) geometries, UT1-2 (resp. NT1-3) were considered for smooth (resp. notched) specimens (Fig. 1b). UT specimens were tested with an elongation rate of $10^{-3}s^{-1}$; a load line displacement velocity of 10^{-3} mm.s^{-1} was used for notched specimens. The gauge length of smooth specimens was 36 mm (resp. 5 mm) for UT1 (resp. UT2). NT2 and NT3 specimen geometries were designed for this study [14], so that specimens could be taken along ND. At 30% of diameter reduction, axial stresses up to 2000 MPa (typical value for cleavage normal to ND) [13] were expected to be found over a region containing both equiaxed and bainitic ferrite. More temperature levels were considered for tests along ND because of the lower amount of literature data along ND (Table 1).

Table 1: Summary of tensile tests, indexed using corresponding specimen geometries

	-196°C	-100°C	-90°C	-80°C	-70°C	-60°C	-55°C	-50°C	-40°C	20°C
RD	NT3	NT1								NT1, UT1
TD	NT3	NT1, UT1								NT1, UT1
ND		NT2, UT2	NT2	NT2	NT2	NT2	NT2	NT2	NT2	NT2, UT2

Elongation of smooth specimens was measured using an extensometer (UT1 geometry) or by applying a stiffness correction on the load vs. load line displacement curve (UT2 geometry). For notched specimens, a radial extensometer was used to measure the reduction of diameter along ND (resp. TD) for specimens taken along RD and TD (resp. along ND). Some tests were (repeatedly) interrupted at room temperature, after which the extensometer was temporarily rotated by 90° with respect to the tensile axis, and the new value of the reduction of diameter was recorded. The ratio of these two values was used as an anisotropy coefficient.

2.3 Observations

Fracture surfaces were observed with scanning electron microscopy (SEM) in secondary electron imaging. This allowed first identification of fracture modes and estimate of the shear percentage, i.e. the ratio of ductile fracture area to the total area of the fracture surface (projected along the tensile axis). Then, cleavage fracture was more quantitatively studied. The propagation path of the first cleavage crack was studied using stereological pairs, 3D reconstruction of the fracture surface (MeX software) together with in-house software to calculate tilt and twist components of misorientation between neighboring facets [15]. Microtexture was analyzed using electron backscatter diffraction (EBSD) on polished sections (190×190 µm²) with a step size of 1 µm. The mean free path of cleavage microcracks was determined by considering crystals with a nearly common orientation of {001} planes normal to the investigated loading axis. The size distribution of such "potential cleavage facets" was compared to the fracture surface appearance.

3 Experimental results

3.1 Tensile tests (smooth and notched specimens)

Figure 2 summarizes the results of the tensile tests, together with the simulated curves. More information on the numerical model can be found in Section 4.The effective stress was calculated as the load divided by the initial cross-section and diameter reduction was normalized by the initial diameter of the minimal section. Test reproducibility was good (difference of stress lower than 5%), so that only one curve per condition is plotted in Fig. 2.

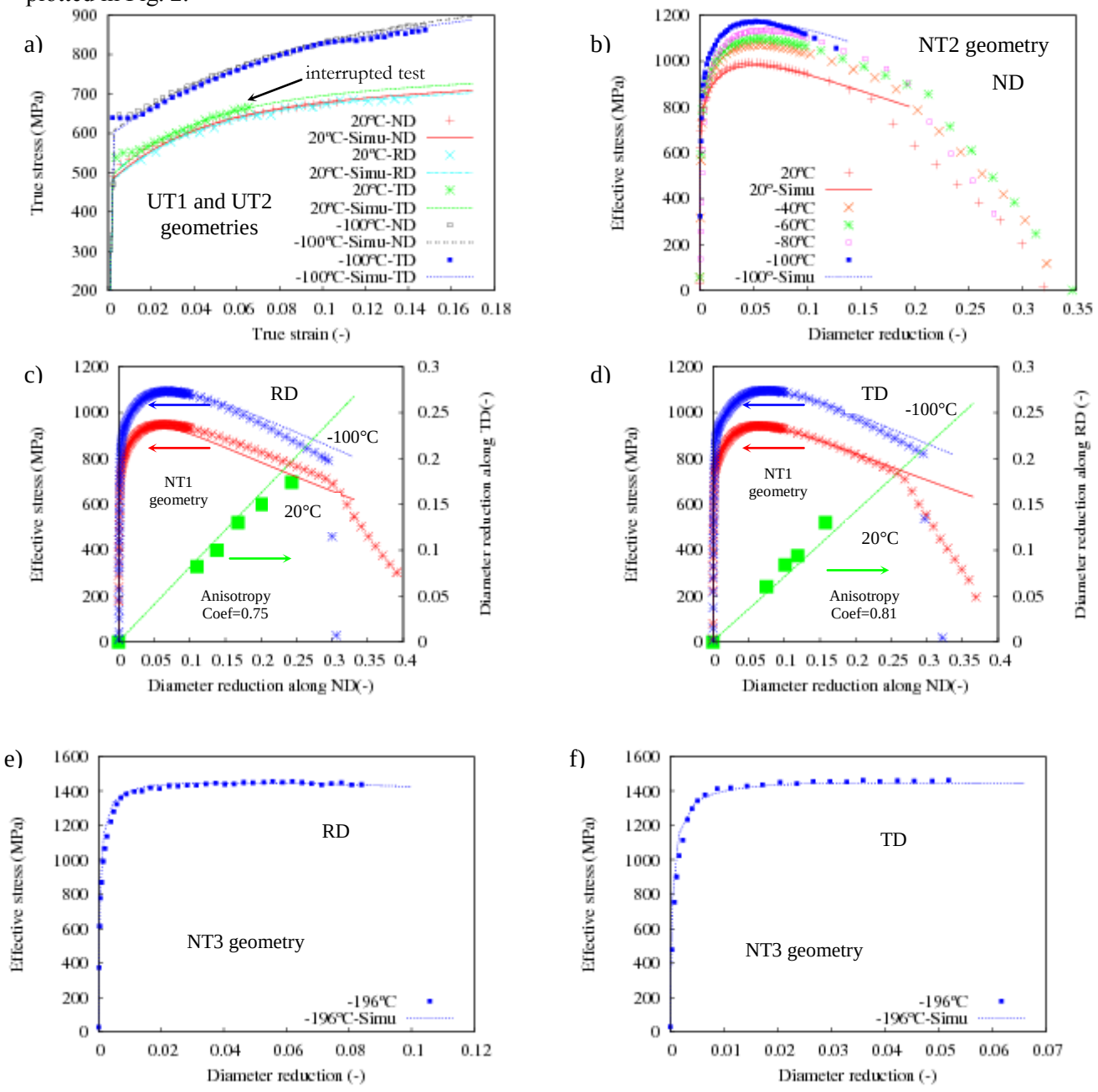

FIG. 2 –Tensile curves of (a) smooth, (b-f) notched specimens. Symbols: experiments; lines: model predictions

Work hardening is higher at -100°C than at 20°C. Anisotropy in strength is not significant but a constant anisotropy coefficient (defined in 2.2), lower than 1, was found along RD and TD (Fig. 2c, 2d). When tested along ND, the minimal section remained circular all along the test (anisotropy ratio equal to 1.0). These curves also showed a brutal drop of the effective stress at the end of tests at -100°C. At this temperature, pop-ins were observed before final failure, in the load vs. load line displacement curves (not shown here).

3.2 Fracture mechanisms

For specimens pulled along RD and TD, three fracture modes were in competition: ductile, delamination and (flat) cleavage fracture. At 20°C, fully ductile fracture was observed. At -100°C, ductile fracture with a central delamination crack was observed (Fig. 3a). At -196°C, flat cleavage cracking, starting far from the notch roots was accompanied with some delamination micro-cracks (Fig. 3b). Specimens tested along ND only exhibited ductile and (flat) cleavage fracture. Three temperature domains were distinguished from these fracture mechanisms: the upper shelf (T > -80°C) with fully ductile fracture, the transition domain (-100°C up to -80°C) with ductile initiation followed by cleavage fracture (Fig. 4a), the lower shelf (T < -100°C) with large cleavage facets elongated along RD. Figure 4b shows that the transition in shear percentage is steeper than the transition in diameter reduction at fracture.

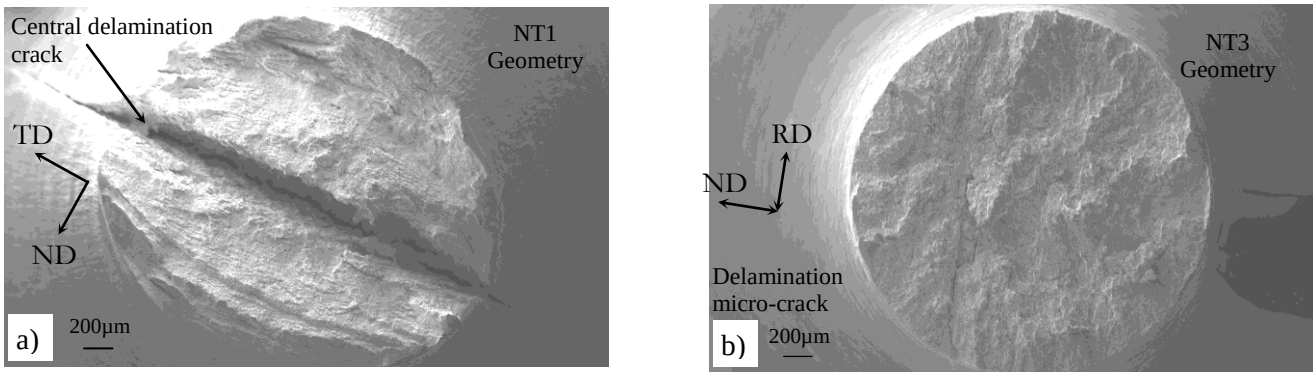

FIG. 3 – Fracture surfaces (a) of a NT1 specimen (RD, -100°C) and (b) of a NT3 specimen (TD, -196°C)

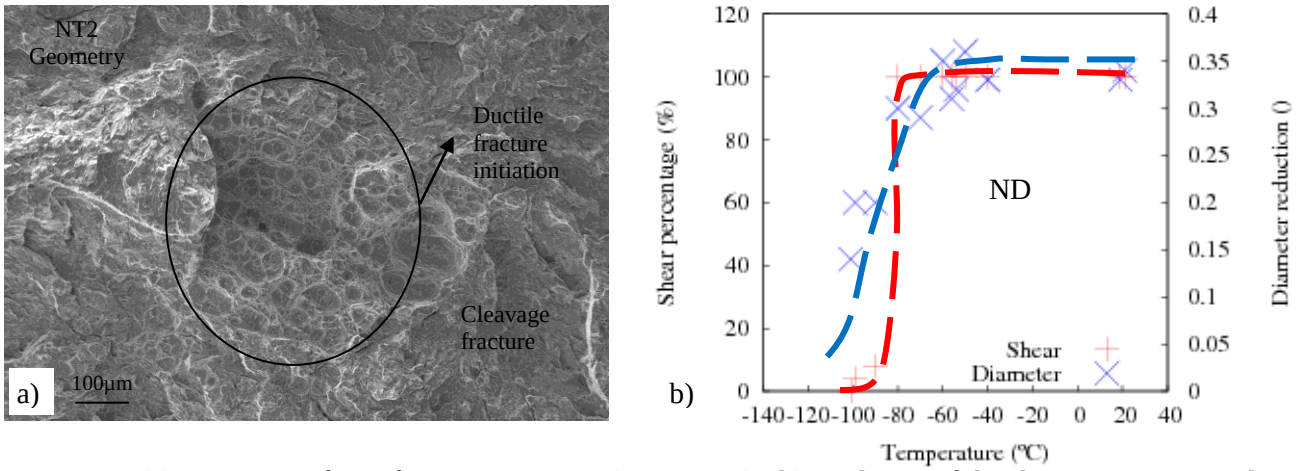

FIG. 4 – (a) Fracture surface of a NT2 specimen (ND, -90°C). (b) Evolution of the shear percentage and diameter reduction (at fracture) with testing temperature (NT2 specimens tested along ND).

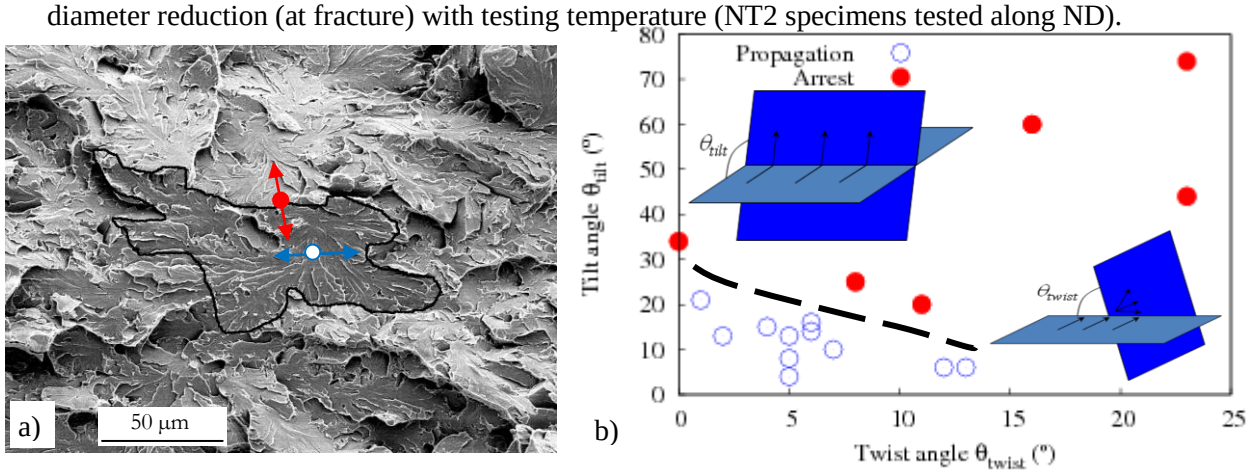

FIG. 5 – (a) Fracture surface of an NT2 specimen tested along ND at -100°C. (b) Local cleavage propagation or arrest according to measured tilt and twist components of misorientation (region delineated in black in (a))

Quantitative fractography was performed on a large facet where cleavage fracture was found to have initiated (Fig 5a). Tilt and twist angles between two neighboring regions across the facet boundary (no direct cleavage crack propagation from one region to the other) and within the considered facet (i.e., with easy cleavage crack propagation between the two regions) are presented in figure 5b. A boundary curve which separates the tilt and twist angles for the propagation of the crack in the same facet, from those which lead to the generation of a new facet was tentatively plotted despite the low number of data for high values of the twist angle. According to that curve, a tilt angle of 20°, or a twist angle up to about 13° (yet with almost no tilt component) was not high enough to arrest cleavage crack propagation. In a first approximation, a misorientation angle of 15° was considered to delimit so-called "potential cleavage facets" from EBSD maps.

3.3 Microtexture

The shape and size of the largest cleavage facets, determined using EBSD in the (RD, TD) plane (Fig. 6) are similar to those of the large elongated cleavage facet of Fig. 5a. From Fig. 6c, cleavage crack initiation could possibly be favored in the delamination plane due to the microtexture of the material.

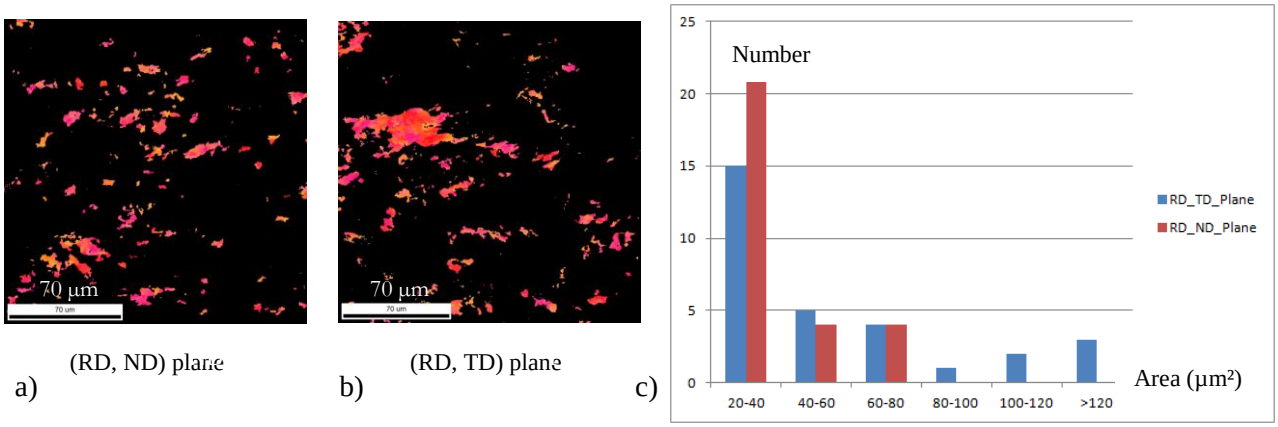

a) (RD, ND) plane b) (RD, TD) plane c)

FIG. 6 – (a,b) Potential cleavage facets using a threshold misorientation angle of 15° between {100} planes and normal to the observed sample plane. (c) Area distribution (in number) of potential cleavage facets

4 Anisotropic cleavage failure criterion

The critical cleavage stress at the onset of fracture of NT specimens was estimated from mechanical analysis. An elastic-plastic constitutive model, with an isotropic hardening rule coupling a linear and an exponential term (Voce equation) was chosen. At 20°C and -100°C, the Bron-Besson anisotropy yield criterion [16] was used. Constitutive parameters were identified from notched and smooth tensile curves along all directions, together with anisotropy coefficients [14]. At -196°C, a von Mises yield criterion was used because of the low number of available results (only two tensile tests on notched specimens). Finite element calculations were performed using quadratic bricks with reduced integration, finite strain formalism, a Newton-Raphson iterative scheme for global convergence and an implicit integration scheme for constitutive equations. After a study of the mesh size effect, a minimum element size at notch root equal to 100µm (ensuring convergence with respect to the mesh size) was considered for calculations. One-eighth of the specimen was modeled and uniform displacement was prescribed at the bottom edge together with usual symmetry conditions. Experimental and predicted curves are in good agreement before the onset of fracture (Figure 3).

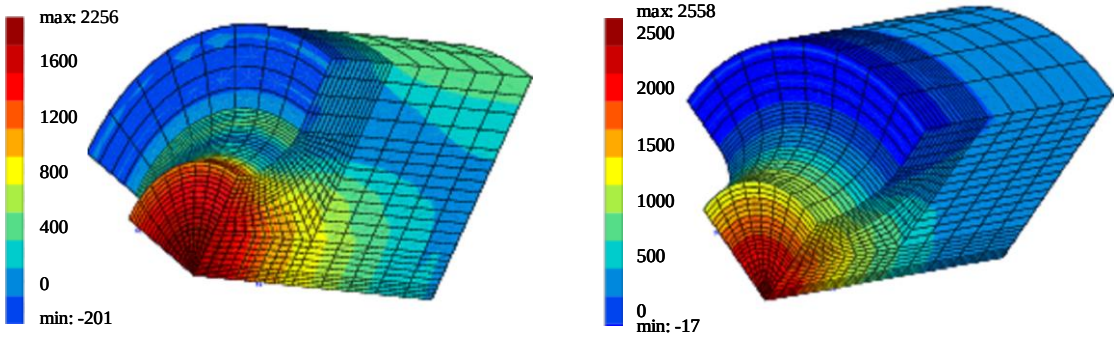

FIG. 7 –Axial stress at fracture (MPa) (a) NT2 specimen (ND, -100°C). (b) NT3 specimen (RD, -100°C).

From axial stress distributions at the onset of fracture (Fig. 7), the value of axial stress was determined at the node corresponding to the experimentally observed cleavage initiation crack site, at -100°C (resp. -196°C) for specimens tested along ND (resp. RD and TD). The critical cleavage stresses obtained are 2010 ±50MPa and 2500 ±100 MPa respectively along ND and RD. The value of this critical stress was not easy to estimate along TD because the fracture surface showed multiple crack initiation sites, and sometimes delamination. The only information extracted from calculations is that the critical stress is at least equal to 2300MPa.

5 Discussion and concluding remarks

NT specimens revealed a strong anisotropy in plastic yield, with easier deformation along ND compared to RD and TD, and also in cleavage fracture. At T > -80°C, ductile fracture occurs whatever the specimen geometry and loading direction. For -100°C < T < -80°C, ductile crack initiation followed by cleavage propagation occurred when pulling along ND. At T < -100°C, cleavage fracture occurred for specimens taken along ND, and delamination cracks (microcracks at -196°C) were still observed for specimens taken along RD and TD. In fact, for temperatures lower than -100°C the stress along ND within the notched specimen become higher than its critical value, which is much lower than that along RD and TD.
From our preliminary EBSD measurements, the rolling plane contains rather large zones susceptible to facilitate the propagation of cleavage cracks by becoming large cleavage facets, in agreement with fractographic observations. Cleavage facets after tension along RD and TD appears smaller, corresponding to small, well-separated zones found with microtexture analysis. More EBSD data are needed to confirm this.
In summary, from tensile tests of notched and smooth specimens in a range of temperature and pulling directions, the occurrence of delamination fracture in a pipeline steel plate has been quantitatively described by an anisotropic critical cleavage stress. This anisotropy seems to be linked to anisotropy in microtexture. Improvement of the resistance of the steel against delamination might be achieved by avoiding the formation of large zones well oriented for cleavage fracture during thermomechanical processing.

6 References

[1] Bramfitt B.L., A study of the delamination behavior of a very low-carbon steel, Metallurgical and Materials Transactions A, 8, 1263-1273, 1977.
[2] Shin Y.S., Separation phenomenon occurring during the Charpy impact test of API X80 pipeline steels, Metallurgical and Materials Transactions A, 40, 2333-2349, 2009.
[3] Inoue T., Delamination effect on impact properties of ultrafine-grained low carbon steel processed by warm caliber rolling, Metallurgical and Materials Transactions A, 41, 341-355, 2010.
[4] Hara T., DWTT properties for high strength line pipe steels, Proceedings of the Eighteenth International Offshore and Polar Engineering Conference, 2008.
[5] Hara T., Effects of microstructure and texture on DWTT properties for high strength line pipe steels, Proceeding of IPC, International Pipeline Conference, 2006.
[6] Fujishiro T., Effects of separation on ductile crack propagation behavior during drop weight tear test, Proceeding of twenty-first international offshore and polar engineering conference, 2011.
[7] Yang Z., Fracture appearance evaluation of high performance pipeline steel DWTT specimen with delamination cracks, Key Engineering Materials, 324-325, 59-62, 2006.
[8] Joo M.S., Role of delamination and crystallography on anisotropy of Charpy toughness in API-X80 steel, Materials Science and Engineering, A 546, 314 -322, 2012.
[9] Yan W., Delamination fracture related to tempering in a high-strength low-alloy steel, Metallurgical and Materials Transactions A, 41, 159-171, 2010.
[10] Mirzaev D.A., Structural aspect of delamination crack formation during the HTMT of steels with a ferritic structure, The physics of metals and metallography, 106, 186-194, 2008.
[11] Yang Z., The Charpy notch impact test of X70 pipeline steel with delamination cracks, Key Engineering Materials, 297-300, 2391-2396, 2005.
[12] Kalyanam S., Delamination cracking in advanced aluminium-lithium alloys-Experimental and computational studies, Engineering fracture mechanics, 76, 2174-2191, 2009.
[13] Baldi G., Critical stress for delamination fracture in HSLA steels, Metal Science, 12, 459-472, 1978.
[14] Tankoua F., ArcelorMittal internal PhD progress report, 2013.
[15] Andrieu A. Multiscale modeling of intergranular fracture in ferritic steels, PhD dissertation, in progress.
[16] Bron F., A yield function for anisotropic materials, application to aluminium alloys, International Journal of Plasticity, 20, 937-963, 2004.